

Demonstration of planar thick InP layers by selective MOVPE

N. Dupuis^{a,*}, J. Décobert^a, P.-Y. Lagrée^b, N. Lagay^a, D. Carpentier^a, F. Alexandre^a

^a Alcatel Thales III-V Lab, Route de Nozay, F-91461 Marcoussis, France

^b CNRS, UPMC Univ Paris 06, IJLRA, F-75005 Paris, France

ARTICLE INFO

Article history:

Received 30 May 2008

Received in revised form

11 July 2008

Accepted 14 July 2008

Available online 3 August 2008

PACS:

81.05.EA

81.15.Gh

keywords:

A3. Metal-organic vapor-phase epitaxy

A3. Selective epitaxy

B2. InP

ABSTRACT

We studied the selective metal-organic vapor-phase epitaxy of thick InP bulk layers. The work focused on the obtention of planar thick layers by an adjustment of the growth conditions. We showed that reduced pressure and temperature in the reactor allowed to decrease the sharpness of the thickness profiles in the vicinity of the mask. This approach is consistent with the vapor phase diffusion model and the kinetic theory. Thick InP layers generally show huge overgrowths at the edges of the dielectric stripes. These overgrowths were suppressed by reducing the growth rate. All samples' thickness profiles were characterized by means of optical interferometer microscopy and surface profiler. Scanning electronic microscopy was used in the observation of the edge overgrowths and highlighted the complexity and anisotropy of the growth at these edges.

© 2008 Elsevier B.V. All rights reserved.

1. Introduction

Selective area growth (SAG) is an important process step for the integration of optoelectronic devices. In SAG, the growth occurs on a wafer partially covered with a dielectric material. As no species can deposit on the amorphous surface of the dielectric, a concentration gradient appears in the vapor phase and the active species diffuse from above the masked areas toward the open areas. Compared with a region far away from any dielectric mask perturbation, the two main effects are thickness enhancement and compositional variations in the case of ternary and quaternary alloys. These two effects are widely used in photonic integrated circuits where a SAG dielectric mask can be tailored in order to integrate different active/passive optical functions. Usually the selectively grown layers are complex stacking including a multiple-quantum well section embedded in separate confinement heterostructures (SCH) and InP layers. The InP buffer layer avoids starting the epitaxial growth directly with a quaternary material, typically the SCH. InP is also commonly used as a spacer for distributed feed back or tunable distributed Bragg reflector lasers. In the SAG regime, the thick InP layers are known to be difficult to handle [1,2]. First, in standard growth conditions, the indium precursor has a very small diffusion length [3] which gives rise to very sharp thickness profiles in the vicinity

of the mask. Second, in the case of thick enough InP layers (300 nm and more), huge overgrowths appear at the edges of the dielectric stripes as shown by Sugiyama et al. [1]. These overgrowths should be suppressed as they can lead to major problems in devices fabrication. In this paper, we focus on the selective area growth conditions of thick InP layers in order to improve the flatness of the thickness profiles and to reduce the overgrowths at the edges.

2. Experiment

All investigated samples were grown in a horizontal AIX200/4 MOVPE reactor, designed for three 2 in wafers using trimethylindium (TMIn), arsine (AsH₃), and phosphine (PH₃) as growth precursors. The InP wafers were pre-processed with 350 nm thick SiO₂ dielectric stripes using conventional plasma enhanced chemical vapor phase deposition (PECVD), photolithography, and reactive ion etching (RIE). The SAG mask layout included various patterns. Basically, the SAG pattern consists of two parallel dielectric stripes aligned with the [110] crystallographic direction. W_m is defined as the width of the stripes and W_o as the opening width between stripes (see inset in Fig. 1). The patterns were very long (900 μm) and sufficiently separated to avoid any influence on each other [4]. The different samples were selectively grown with various temperature and pressure conditions which will be described latter in the paper. Different growth rates were also investigated by changing the input TMIn flow rate at constant

* Corresponding author.

E-mail address: nicolas.dupuis@3-5lab.fr (N. Dupuis).

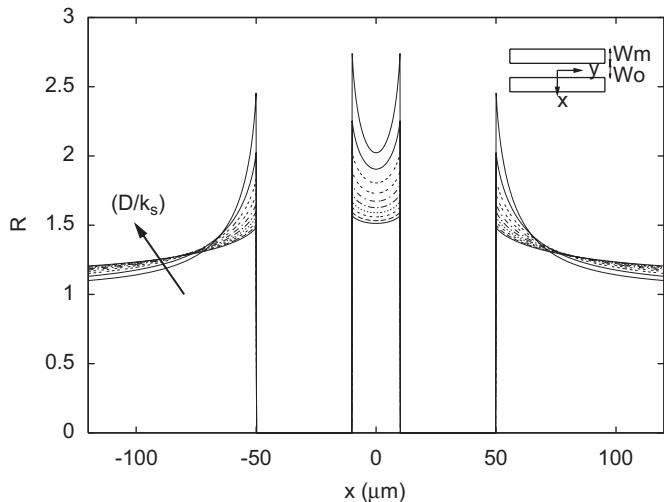


Fig. 1. Calculations in VPD of the growth rate enhancement R along x direction with (D/k_s) varied from 10 to 100 μm every 10 μm steps. W_m is fixed to 40 μm and W_o to 20 μm . The calculations show the evolution of the R profile which goes smoother (see arrow) while increasing (D/k_s) .

PH_3 flow (100 sccm). In the field region (i.e. far away from any mask perturbation), all the investigated samples had the same thickness sequence that is a 97 nm InP/ 3 nm InAsP stack repeated seven times leading to a global thickness of 700 nm. The markers were added for convenience with scanning electronic microscopy (SEM) observations. In order to characterize the thickness profiles around the mask, both optical interferometer microscopy (OIM) and surface profiler have been used, the latter one being much more adapted to precisely measure the overgrowths at the edges of the mask.

3. Results and discussion

In selective epitaxy, the shape of the concentration profiles around the mask is known to be strongly dependent on the growth conditions [5–8]. As a first approximation, the vapor phase diffusion (VPD) model is well adapted to calculate the concentration profiles around any masked areas [6,9]. In this model, the diffusion equation $D\nabla^2 N = 0$ is solved with the proper boundaries on the mask, $\partial N/\partial z = 0$, and on the crystal, $D\partial N/\partial z = k_s N$. The former boundary condition on the flux implies a perfect selectivity that is no deposition on the mask. The second one is a mixed condition which states the equilibrium between the reaction on the wafer and the incident flow. It also introduces the main driving parameter of the model namely the (D/k_s) parameter. D ($\text{m}^2 \text{s}^{-1}$) is the diffusion coefficient of the reactants in the vapor phase and k_s (m s^{-1}) a sticking rate constant which depends on the reactivity of source molecules on the crystal surface. Therefore, (D/k_s) expresses an effective diffusion length and is commonly expressed in μm . As an example, Fig. 1 shows different concentration profiles along a cross section of the mask (x axis, see inset on Fig. 1) extracted from VPD calculations with various D/k_s values. These calculations were realized for $W_m = 40 \mu\text{m}$ and $W_o = 20 \mu\text{m}$. The profiles were normalized to the far field reference to get the growth rate enhancement (R). As seen in Fig. 1, short (long) D/k_s give rise to sharp (extended) profiles. The operating conditions (p and T) will have an influence on both D and k_s . The D coefficient can be evaluated from kinetic theory and one can easily show that $D \propto (k_B T)^{3/2}/p\sigma^2$ with k_B the Boltzmann constant, T the temperature, p the pressure and σ the collision diameter of the diffusing molecule. The k_s rate constant is a

median macroscopic constant which involves many different chemical reactions and cannot be easily expressed. This constant will mainly depend on the growth temperature.

Clearly, in the SAG regime, a first step to improve the flatness and decrease the sharpness of the thickness profiles is to obtain a large D/k_s for a given diffusing precursor. We now compare two different thick InP layers in two different growth conditions (GC). In GC₁ (GC₂) the growth temperature was set to 650 °C (590 °C) and the reactor pressure to $p = 150$ mbar ($p = 50$ mbar). For both conditions, good morphology and high selectivity on the mask were observed. Fig. 2 sketches measured thickness profiles along x direction with OIM setup for the two different growth conditions: GC₁ (a) and GC₂ (b). The VPD model was used to fit the experimental profiles and to deduce the characteristic diffusion lengths D/k_s of each GC. The extracted values, $(D/k_s)_1 = 10 \mu\text{m}$ and $(D/k_s)_2 = 90 \mu\text{m}$, clearly show the strong influence of the reactor pressure and temperature. The reduced pressure and temperature in GC₂ increase D/k_s and as a consequence improve the flatness of the concentration around the mask. This explains the strong decrease of the thickness profiles sharpness in the vicinity of the dielectric, as seen on (b) profiles. The reduced pressure is consistent with an increase of the mean-free path of the molecules which lead to a faster diffusion process (higher D). The main effect of the reduced temperature is the decrease of molecules reactivity (smaller k_s) on the crystal surface. Note that

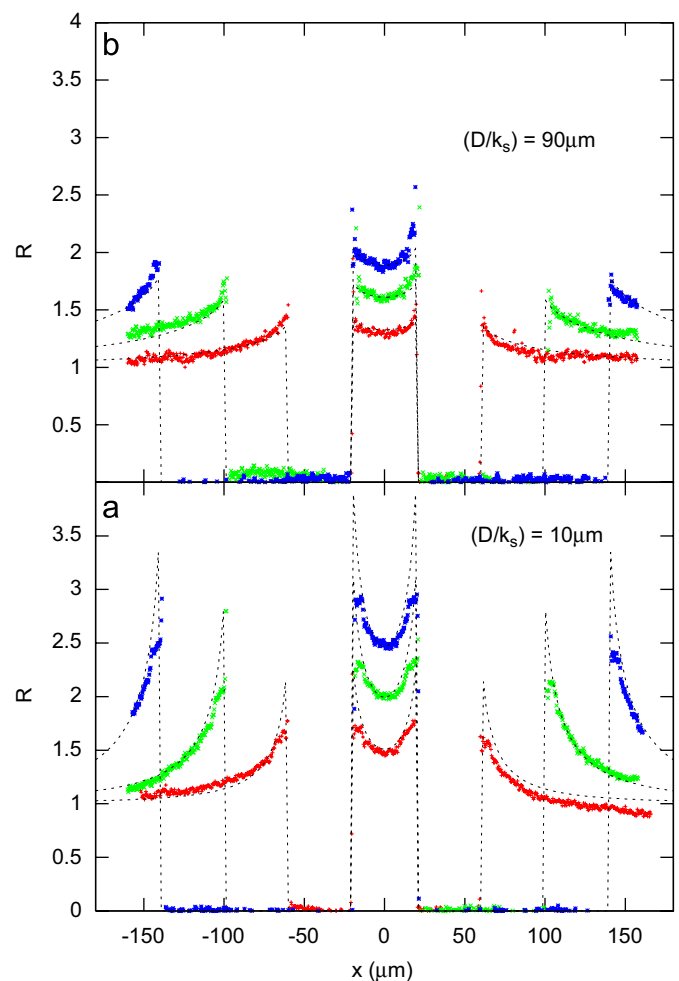


Fig. 2. InP growth rate enhancement fitting (dots) with VPD model (dashed lines) for two growth conditions: (a) GC₁ and (b) GC₂; in both cases, the fit is repeated for three mask widths $W_m = 40/80/120 \mu\text{m}$; the opening W_o is kept constant, $W_o = 40 \mu\text{m}$.

the temperature decrease will also naturally affect D and at least reduce it. However, comparing the ranges $p = 150\text{--}50\text{ mbar}$ and $T = 650\text{--}590^\circ\text{C}$, one easily convinces himself that the reduced temperature will have a negligible effect on D compared with the reduced pressure. Kinetic theory gives the relation between D_1 and D_2 and as a consequence the relation between k_{s1} and k_{s2} . Assuming that for both growth conditions, the same growth precursors diffuse in the vapor phase we have

$$\frac{D_1}{D_2} \approx \left(\frac{T_1}{T_2}\right)^{3/2} \left(\frac{p_2}{p_1}\right) = 0.4 \quad (1)$$

then

$$\frac{k_{s1}}{k_{s2}} \approx 3.3 \quad (2)$$

As seen with Eqs. (1) and (2), the pressure and temperature adjustments have a strong effect on both coefficients D and k_s . From GC₁ to GC₂, D is increased by 50% while k_s is decreased by about 70%. Oh et al. found similar results in a study concerning (D/k_s) dependence on growth temperature and pressure for GaAs in SAG [10]. It should be noted that the ratio found from Eq. (2) cannot be used to calculate an activation energy for the TMIn precursor since the partial pressure was not the same in GC₁ and GC₂ ($p_{\text{TMIn}(1)} \approx 3p_{\text{TMIn}(2)}$). VPD and kinetic theory show the advantages of low pressure/temperature in the case of InP growth.

At the dielectric's edges, the situation is much more complicated. The adjustment of the growth temperature and the reactor pressure was not effective to suppress the huge overgrowths. Note that these overgrowths were not observable with OIM setup (Fig. 2) because of the small lateral resolution of this technique ($\approx 1.5\ \mu\text{m}$ for $\times 20$ magnification) and therefore were measured with the surface profiler. The edge overgrowths were found to depend strongly on the growth rate. In Fig. 3, we present measurements of the overgrowths along the $[01\bar{1}]$ crystallographic direction (x -axis) for two different field growth rates $v_1 = 0.4\ \text{nm/s}$ (a) and $v_4 = 0.1\ \text{nm/s}$ (b). The growth temperature and reactor pressure were the same as in GC₂. In both cases (a) and (b), the measurement was repeated for several Wm configurations while the opening width W_o was kept equal to $40\ \mu\text{m}$. The high growth rate v_1 (a) leads to huge overgrowths especially for large Wm while in the case of v_2 (b), planar profiles were observed. Another convenient way to observe these results is to plot the overgrowth dependence with Wm (Fig. 4) for different growth rates: $v_1 = 0.4\ \text{nm s}^{-1}$, $v_2 = 0.3\ \text{nm s}^{-1}$, $v_3 = 0.2\ \text{nm s}^{-1}$ and $v_4 = 0.1\ \text{nm s}^{-1}$. In Fig. 4, the edge overgrowth thickness (h_e) is normalized to the center thickness measured between the two dielectric stripes (h_c) at $x = y = 0$ leading to $OG = (h_e/h_c) - 1$, as detailed in the Fig. 4 inset. The Wm comparison is interesting since the growth rate enhancement in the vicinity of the masked area is known to have a linear dependence with Wm (see Ref. [6]). As a consequence, in the VPD model the ratio h_e/h_c should theoretically be a constant. The increase of OG with both v and Wm shows the development of the overgrowth. As an example, with $Wm = 230\ \mu\text{m}$ and v_4 , the overgrowth is $\approx 150\%$ of the total thickness measured between the two dielectric stripes. This corresponds to an overgrowth of up to $2\ \mu\text{m}$ at the edges of the dielectric (see Fig. 3). Fig. 4 clearly shows that only the lower growth rate v_4 avoids the edge overgrowth development over the whole Wm range. Similar results were observed in the $[110]$ crystallographic direction from $Wm = 20$ to $100\ \mu\text{m}$. The dependence of OG with the growth rate was slightly different but the lower growth $v_4 = 0.1\ \text{nm s}^{-1}$ also gives rise to planarized profiles. For larger Wm , we observed that OG begins to increase with Wm . For the moment, we do not have a clear explanation of this phenomena. Due to its simplicity, VPD model cannot precisely fit the thickness in the vicinity of the mask [6] and explain the edge

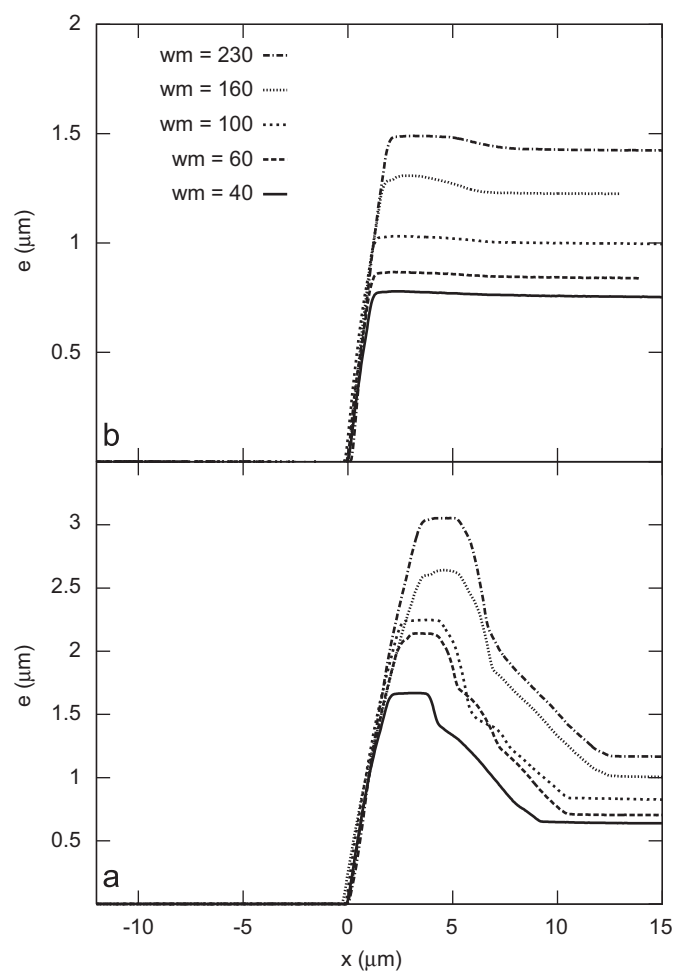


Fig. 3. Surface profiling along x direction at the edges of the mask for two different growth rates: (a) $v = 0.4\ \text{nm/s}$ and (b) $v = 0.1\ \text{nm/s}$. For each growth rate, different mask widths are depicted: $Wm = 40/60/100/160/230\ \mu\text{m}$. The opening between masked stripes is $W_o = 40\ \mu\text{m}$.

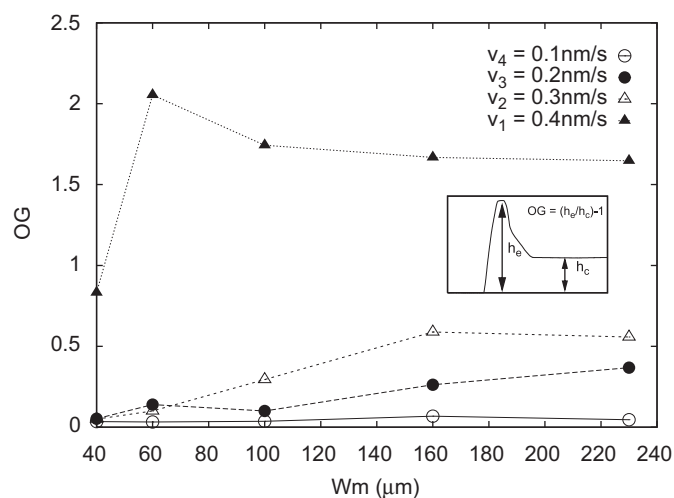


Fig. 4. Normalized edges overgrowth (OG) measured with the surface profiler against the mask width Wm for different growth rates. The opening between masked stripes is $W_o = 40\ \mu\text{m}$.

overgrowths. To accurately fit these edges the model should include non-stationary boundaries, surface diffusion on both crystal and masked areas [1]. Cross sections of mask edges were

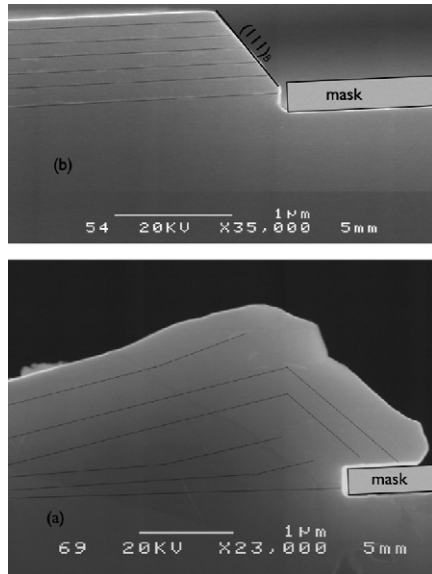


Fig. 5. SEM cross sections of mask edges for two different growth rates: (a) $v = 0.4$ nm/s and (b) $v = 0.1$ nm/s. Thin lines are superposed with the InAsP markers to guide the eyes. The SAG mask ($W_m = 160$ μm and $W_o = 40$ μm) is also depicted.

also observed with SEM. In Fig. 5 are shown the samples corresponding to GC_2 with v_1 (a) and v_4 (b). The SAG mask geometry was in this case set to $W_m = 160$ μm and $W_o = 40$ μm . To guide the eyes, thin lines follow the InAsP markers and show the surface shape evolution. In the (a) cross section, the growth is very perturbed and complex anisotropy and crystallographic facets are revealed.

One can notice at least two different typical points. First is the huge overgrowth in the vicinity of the mask. This overgrowth agrees with the surface profiler edge measurements discussed above (see Fig. 3(a) for $W_m = 160$ μm). The second point concerns the lateral growth which appears over the mask and can be very problematic in the case of device fabrication. For example, a technology step with photoresist and dielectric deposition

followed by classical lithography and RIE will be difficult to handle. Indeed the dielectric material will be localized above the lateral overgrowth which makes it difficult to remove. In the case of (b) cross section no overgrowths and no lateral growth are observed. The profile is planar and one can observe the development of the $(111)_B$ typical facet at the edge of the mask.

4. Conclusion

We investigated different selective growth conditions to obtain planar thick InP layers. In order to improve the flatness and reduce the sharpness of the thickness profiles we tuned the temperature and pressure ranges to have a larger D/k_s parameter. This approach relied on a simple VPD approach and kinetic theory arguments. Thick selectively grown InP layers also showed some typical huge overgrowths at the edges of the dielectric. We studied the evolution of this overgrowth with the SAG mask width and showed that a reduced growth speed almost suppressed it. This work proposed a valuable step to obtain planar thick InP layers and can reasonably offer a key to simplify the devices technological post-processing.

References

- [1] M. Sugiyama, N. Waki, Y. Nobumori, H. Song, T. Nakano, T. Arakawa, Y. Nakano, Y. Shimogaki, J. Crystal Growth 287 (2005) 668.
- [2] T. Shioda, M. Sugiyama, Y. Shimogaki, Y. Nakano, J. Crystal Growth 298 (2007) 37.
- [3] J. Décobert, N. Dupuis, P.Y. Lagrée, N. Lagay, A. Ramdane, A. Ougazzaden, F. Poingt, C. Cuisin, C. Kazmierski, J. Cryst. Growth 298 (2007) 28.
- [4] N. Dupuis, J. Décobert, P.-Y. Lagrée, N. Lagay, F. Poingt, C. Kazmierski, A. Ramdane, A. Ougazzaden, J. Appl. Phys. 103 (2008).
- [5] M.-S. Kim, C. Caneau, E. Colas, R. Bhat, J. Crystal Growth 123 (1992) 69.
- [6] M. Gibbon, J.-P. Stagg, C.-G. Cureton, E.-J. Thrush, C.-J. Jones, R.-E. Mallard, R.-E. Pritchard, N. Collis, A. Chew, Semicond. Sci. Technol. 8 (1993) 998.
- [7] T. Fujii, M. Ekawa, S. Yamazaki, J. Crystal Growth 156 (1995) 59.
- [8] M. Ida, N. Shigekawa, T. Furuta, H. Ito, T. Kobayashi, J. Crystal Growth 158 (1996) 437.
- [9] M.-A. Alam, et al., Appl. Phys. Lett. 74 (1999) 2617.
- [10] H.-J. Oh, M. Sugiyama, Y. Nakano, Y. Shimogaki, Jpn. J. Appl. Phys. 42 (2003) 6284.